ResearchGate

See discussions, stats, and author profiles for this publication at: https://www.researchgate.net/publication/322566826

Novel Approach for In Vivo Detection of Vulnerable Coronary Plaques Using Molecular 3-T CMR Imaging With an Albumin-Binding Probe

Article *in* JACC. Cardiovascular imaging · January 2018

DOI: 10.1016/j.jcmg.2017.10.026

CITATIONS
4

READS
100

15 authors, including:

Leif-Christopher Engel
Deutsches Herzzentrum München
45 PUBLICATIONS **459** CITATIONS

SEE PROFILE

Ulf Landmesser
Charité Universitätsmedizin Berlin
575 PUBLICATIONS **25,194** CITATIONS

SEE PROFILE

Milosz J. Jaguszewski
Medical University of Gdansk
196 PUBLICATIONS **1,709** CITATIONS

SEE PROFILE

Carsten Skurk
Charité Universitätsmedizin Berlin
117 PUBLICATIONS **5,051** CITATIONS

SEE PROFILE

Some of the authors of this publication are also working on these related projects:

Non-Invasive, MRI-Based Calculation of the Aortic Blood Pressure Waveform Using Computational Fluid Dynamics View project

Sabiniewicz Robert View project

All content following this page was uploaded by Leif-Christopher Engel on 30 January 2018.

The user has requested enhancement of the downloaded file.

JACC: CARDIOVASCULAR IMAGING
VOL. ■, NO. ■, 2018
© 2018 BY THE AMERICAN COLLEGE OF CARDIOLOGY FOUNDATION
ISSN 1936-878X/$36.00
PUBLISHED BY ELSEVIER
https://doi.org/10.1016/j.jcmg.2017.10.026

Novel Approach for In Vivo Detection of Vulnerable Coronary Plaques using Molecular 3-T CMR Imaging with an Albumin-Binding Probe

Leif-Christopher Engel, MD,[a,b] Ulf Landmesser, MD,[a,b,c] Kevin Gigengack, MS,[a] Thomas Wurster, MD,[a] Constantina Manes, MD,[a] Georg Girke, MD,[a] Milosz Jaguszewski, MD,[a] Carsten Skurk, MD,[a] David M. Leistner, MD,[a] Alexander Lauten, MD,[a] Andreas Schuster, MD, PhD, MBA,[d,e] Bernd Hamm, MD,[h] Rene M. Botnar, PhD,[f,g] Marcus R. Makowski, MD, PhD,[h] Boris Bigalke, MD, MBA[a]

ABSTRACT

OBJECTIVES This study sought to investigate the potential of the noninvasive albumin-binding probe gadofosveset-enhanced cardiac magnetic resonance (GE-CMR) for detection of coronary plaques that can cause acute coronary syndromes (ACS).

BACKGROUND ACS are frequently caused by rupture or erosion of coronary plaques that initially do not cause hemodynamically significant stenosis and are therefore not detected by invasive x-ray coronary angiography (XCA).

METHODS A total of 25 patients with ACS or symptoms of stable coronary artery disease underwent GE-CMR, clinically indicated XCA, and optical coherence tomography (OCT) within 24 h. GE-CMR was performed approximately 24 h following a 1-time application of gadofosveset-trisodium. Contrast-to-noise ratio (CNR) was quantified within coronary segments in comparison with blood signal.

RESULTS A total of 207 coronary segments were analyzed on GE-CMR. Segments containing a culprit lesion in ACS patients ($n = 11$) showed significant higher signal enhancement (CNR) following gadofosveset-trisodium application than segments without culprit lesions ($n = 196$; 6.1 [3.9 to 16.5] vs. 2.1 [0.5 to 3.5]; $p < 0.001$). GE-CMR was able to correctly identify culprit coronary lesions in 9 of 11 segments (sensitivity 82%) and correctly excluded culprit coronary lesions in 162 of 195 segments (specificity 83%). Additionally, segmented areas of thin-cap fibroatheroma ($n = 22$) as seen on OCT demonstrated significantly higher CNR than segments without coronary plaque or segments containing early atherosclerotic lesions ($n = 185$; 9.2 [3.3 to 13.7] vs. 2.1 [0.5 to 3.4]; $p = 0.001$).

CONCLUSIONS In this study, we demonstrated for the first time the noninvasive detection of culprit coronary lesions and thin-cap fibroatheroma of the coronary arteries in vivo by using GE-CMR. This method may represent a novel approach for noninvasive cardiovascular risk prediction. (J Am Coll Cardiol Img 2018;■:■–■) © 2018 by the American College of Cardiology Foundation.

From the [a]Klinik für Kardiologie, Charité Campus Benjamin Franklin, Universitätsmedizin Berlin, Berlin, Germany; [b]Berlin Institute of Health, Berlin, Germany; [c]DZHK (German Centre for Cardiovascular Research), Partner Site, Berlin, Germany; [d]Department of Cardiology, Royal North Shore Hospital, The Kolling Institute, Northern Clinical School, University of Sydney, Sydney, Australia; [e]Department of Cardiology and Pulmonology, German Centre for Cardiovascular Research Deutsches Zentrum für Herz-Kreislauf-Forschung e.V. (DZHK) Partner Site, Göttingen, Germany; [f]Division of Imaging Sciences and Biomedical Engineering, King's College London, London, United Kingdom; [g]Pontificia Universidad Católica de Chile Escuela de Ingeniería, Santiago, Chile; and the [h]Klinik für Radiologie, Charité Campus Benjamin Franklin, Universitätsmedizin Berlin, Berlin, Germany. Dr. Makowski has received financial support from Deutsche Forschungsgemeinschaft grant 5943/31/41/91. Dr. Botnar was supported by British Heart Foundation grants PG/10/044/28343 and RG/12/1/29262. Dr. Engel is a participant in the Berlin Institute of Health Charité Clinician Scientist Program funded by Charité-Universitätsmedizin Berlin and Berlin Institute of Health. All other authors have reported that they have no relationships relevant to the contents of this paper to disclose. Drs. Engel and Landmesser contributed equally to this work and are joint first authors. Drs. Makowski and Bigalke contributed equally to this work, and are joint senior authors.

Manuscript received July 26, 2017; revised manuscript received October 18, 2017, accepted October 18, 2017.

ABBREVIATIONS AND ACRONYMS

ACS = acute coronary syndrome

CAD = coronary artery disease

CMR = cardiac magnetic resonance

CNR = contrast-to-noise ratio

GE-CMR = gadofosveset-enhanced cardiac magnetic resonance

NSTEMI = non-ST-segment elevation myocardial infarction

OCT = optical coherence tomography

PCI = percutaneous coronary intervention

TCFA = thin-cap fibroatheroma

XCA = x-ray coronary angiography

Acute coronary syndromes (ACS) are largely caused by coronary atherosclerotic plaque rupture or erosion (1). Vulnerable plaques are frequently classified as thin-cap fibroatheroma (TCFA) that often do not cause significant stenosis and have distinct characteristics such as a large necrotic core with an overlying thin intact fibrous cap, macrophage infiltration, and an increased number of structurally compromised intraplaque neovessels (2,3). Molecular imaging using targeted probes offers novel possibilities to better understand molecular events that underlie coronary plaque formation and, thus, has high potential to become a valuable tool for early detection of coronary atherosclerosis (4–6). The albumin-binding probe gadofosveset-trisodium investigated in this study is a clinically approved target-specific molecular cardiac magnetic resonance (CMR) probe (7,8). This gadolinium-based probe reversibly binds to serum albumin, resulting in a significantly prolonged serum half-life (mean ± SD half-life of the elimination phase is 16.3 ± 2.6 h) and a 5- to 10-fold increase in T1 relaxivity. Gadofosveset behaves similarly to Evan's blue dye, a marker of endothelial permeability, and accumulates within the matrix of atherosclerotic plaques (7,8).

The aim of this study was to investigate the clinical potential of gadofosveset-enhanced cardiac magnetic resonance (GE-CMR) as a novel in vivo biomarker for detection of culprit lesions in patients presenting with ACS and for detection of TCFA as confirmed by invasive x-ray coronary angiography (XCA) and optical coherence tomography (OCT) (Ilumien system, St. Jude Medical, Minnesota St. Paul, Minnesota).

METHODS

STUDY POPULATIONS. The study was approved by the local ethics committee for clinical investigations and was performed in accordance with the Declaration of Helsinki. All patients provided written informed consent. Between April 2015 and May 2016, we enrolled overall 25 patients with symptoms of stable coronary artery disease (CAD) (n = 16) and ACS (n = 2 unstable angina and n = 7 non-ST-segment elevation myocardial infarction [NSTEMI]), as defined by the current guidelines of the European Society of Cardiology (9). Hemodynamically unstable patients such as patients with cardiogenic shock, significant cardiac arrhythmia, or rising cardiac heart enzymes were excluded from the study. Additional exclusion criteria involved renal insufficiency (creatinine clearance <30 ml/min), pregnant women, patients with a history of percutaneous coronary interventions, including stent implementation; patients with mental disorders or inability to give consent; patients <18 years of age; and common contraindications to cardiac magnetic resonance imaging (i.e., gadolinium-based contrast agents, claustrophobia, specific metallic items such as cochlear implants, central nervous system aneurysm clips, and pacemakers or defibrillators). GE-CMR was performed successfully in all patients within 24 h prior to undergoing XCA and OCT.

CMR. All scans were done with the subjects in the supine position, using a 3-T CMR (Magnetom Skyra, Siemens Healthcare, Erlangen, Germany), using an 18-channel matrix coil. Following the acquisition of scout scans to identify the major structures of the heart, a cine 4-chamber view was used to determine trigger delay and acquisition window, followed by a TI scout to determine the patient-specific inversion time to null signal from blood. Whole-heart CMR coronary angiography was performed using a T2-prepared fast low-angle shot (FLASH) sequence for the nulling of signal from muscles and veins and a fat saturation pulse for the nulling of signal from fatty tissues. Whole-heart coronary vessel wall imaging was performed using an inversion recovery (IR) prepared 3-dimensional (3D) T1-weighted turbo FLASH sequence with fat suppression (fat saturation [FatSat]). CMR imaging was performed twice: prior to a baseline examination (noncontrast) and approximately 24 h following a one-time application of gadofosveset-trisodium (GE-CMR). Scan parameters (Online Appendix) of the baseline CMR examination and GE-CMR were identical. However, the inversion time was specifically adjusted based on the TI scout to null the signal from blood in the pre-contrast and post-contrast scan.

XCA AND OCT. All subjects were sent to an interventional catheterization laboratory (Allura Xper FD20 laboratory, Phillips, Baltimore, Maryland) after noninvasive CMR and XCA were performed according to standard techniques, using a transradial or transfemoral approach. At least 2 orthogonal views were acquired for all coronary arteries. Following the XCA procedure, OCT of the culprit coronary artery was performed. In case of absence of significant stenosis (stenosis >50%) on conventional XCA. OCT scans were obtained in the vessel with the largest amount of coronary plaques. The radiopaque distal marker of the OCT system was positioned 1 to 2 cm distal to the culprit lesion and iodinated contrast agent (Imeron)

was injected by an automatic pump system (Angiomat Illumena, Liebel-Flarsheim, Austin, Texas). Acquired OCT datasets were transferred in DICOM format for offline analysis.

OCT IMAGE ANALYSIS. OCT frames were evaluated by 2 experienced readers (M.J. and L.-C.E.), who were first blinded to the CMR datasets, by using proprietary software (ILUMIEN OPTIS PCI Optimization System, St. Jude Medical). Consensus reading was performed by a third investigator (B.B.) in case of disagreement between the 2 OCT readers. Plaques were evaluated using validated OCT criteria (10,11). A TCFA was considered a vulnerable plaque defined as a plaque with cap thickness <65 μm and a lipid-rich core with a lipid arc of >90°. Cap thickness was measured 3 times at the site of minimal thickness, and the mean value was calculated. Using the abovementioned criteria, coronary plaques were divided as follows into 6 types according to plaque vulnerability, according to Cheng et al. (12): 1) fibrotic plaque (consisting predominantly of fibrous tissue without confluent lipid core or dense calcium); 2) fibrocalcific plaque (presence of >10% confluent dense calcium without confluent lipid core); 3) fibroatheroma (presence of >10% confluent lipid core with an overlying layer of fibrous tissue); 4) calcified fibroatheroma (fibroatheroma containing 10% confluent dense calcium); 5) noncalcified TCFA (presence of >10% confluent lipid core in direct contact with the lumen, lipid arc >90°; cap thickness <65 um); and 6) calcified TCFA (TCFA containing >10% confluent dense calcium; calcified plaque component in close proximity of <5 mm to TCFA).

Stable plaques were defined as fibrotic plaques, fibrocalcific plaques, or fibroatheroma or calcified fibroatheroma (types I to IV).

CMR IMAGE ANALYSES. For qualitative and quantitative image analysis, CMR data sets were processed with dedicated image analysis software (Osirix software version 3.6.1, Pixmeo, Geneva, Switzerland). As described previously (13), coronary wall and coronary lumen data sets were automatically fused comparably to that in positron emission tomography-computed tomography to spatially colocalize coronary wall contrast enhancement with the course of the coronary arteries (CMR angiogram). All CNR measurements were performed in 9 different coronary segments (proximal, mid, distal RCA; left main; proximal, mid and distal LAD; and proximal and distal LCX). Contrast-to-noise ratio (CNR) was obtained by dividing the difference in signal intensity (SI) between the coronary lesion and blood by the background noise, that is, (SI lesion - SI blood)/noise). Background noise was defined as the SD of the SI in a region of interest placed ventrally to the patient's chest wall.

CNR ANALYSIS I: OCT INFORMED THE LOCATION OF VULNERABLE PLAQUE ON GE-CMR. After OCT image analysis, the exact location of a culprit coronary lesion or TCFA, respectively, was revealed to all CMR readers (L.-C.E. and K.G.), and thorough co-registration between GE-CMR and OCT was performed using anatomical landmarks such as vessel branch points, including distance measurements. CNR were performed in all segments (segments with and without the presence of a TCFA or culprit ACS lesion).

CMR ANALYSIS II: BLINDED ANALYSIS FOR IDENTIFICATION OF CULPRIT ACS LESIONS. In a subsequent analysis, CNR measurements were performed on all pseudonymized CMR data sets, which were given to the CMR reader (L.-C.E.) in a random fashion. During CMR analysis II, the reader (L.-C.E.) was blinded and had no access to the corresponding XCA and OCT findings. After completion of the CNR analysis of all available coronary segments, CNRs of all coronary segments were compared to the findings of the invasive procedures.

STATISTICS. For statistical analysis, SPSS version 24 software (SPSS Statistics, IBM, Armonk, New York) was used. Results are expressed as mean ± SD or median (range) for non-normally distributed data. An unpaired Student *t* test and Mann-Whitney *U* test was applied for comparison of continuous and non-normally distributed variables, respectively. Categorical variables were compared by the chi-square test. Receiver operating characteristic (ROC) analysis was performed to determine diagnostic accuracy for the identification of vulnerable plaques and to determine the optimum CNR cutoff value of GE-CMR for identification of culprit coronary lesions and TCFA. Selection of the optimal cutpoint was based on the Youden index (i.e., the maximum sum of sensitivity and specificity). No adjustments were made for multiple observations within individuals. All tests were 2-sided, and a p value of <0.05 was considered statistically significant.

RESULTS

Clinical and angiographic characteristics are shown in **Tables 1 and 2**, respectively.

CMR ANALYSIS. Of 225 coronary segments, 207 were included for analysis on GE-CMR.

Eighteen coronary segments of a total of 9 patients had to be excluded due to insufficient image quality. The excluded segments were mainly located distally

TABLE 1 Baseline Patients' Characteristics and Medical Treatment on Admission

	Patients With ACS (n = 9)	Patients Without ACS (n = 16)	p Value
Age, yrs	74.6 ± 11.7	67.4 ± 13.1	0.09
Men	5 (55.6)	11 (68.8)	0.51
Weight, kg	77.5 ± 21.9	83.6 ± 18.7	0.25
BMI, kg/m^2	26.7 ± 8.0	28.1 ± 5.0	0.29
Risk factors			
Hypercholesterolemia	3 (33.3)	9 (56.3)	0.27
Hypertension	8 (88.9)	13 (81.3)	0.62
Diabetes mellitus	3 (33.3)	4 (25.0)	0.66
Smokers	3 (33.3)	8 (50.0)	0.42
Family history of CAD	2 (22.2)	3 (18.8)	0.83
Laboratory findings			
Troponin T, ng/ml	78.5 (44.8-346.8)	7.0 (3.0-18.0)	**0.005***
CK, UI/l	167.9 ± 67.7	133.1 ± 122.9	0.22
CK-MB, UI/l	34.9 ± 27.8	27.2 ± 33.7	0.29
Creatinine, mg/dl	1.0 ± 0.3	1.0 ± 0.3	0.31
C-reactive protein, mg/dl	6.1 (4.4-19.8)	6.5 (5.0-25.0)	0.48
Platelets, ×10^9	267.9 ± 48.0	237.1 ± 55.0	0.09
Total cholesterol, mg/dl	163.8 ± 43.1	188.9 ± 47.6	0.11
Triglyceride, mg/dl	137.3 ± 66.0	176.3 ± 122.9	0.20
HDL cholesterol, mg/dl	46.8 ± 16.3	44.0 ± 11.1	0.31
LDL cholesterol, mg/dl	93.6 ± 37.7	122.9 ± 44.1	0.05
Hemoglobin A_{1c}, %	6.6 ± 1.2	6.1 ± 0.7	0.11
Medication			
Aspirin	6 (66.6)	10 (62.5)	0.83
Clopidogrel	2 (22.2)	1 (6.3)	0.24
Statin	4 (44.4)	5 (31.3)	0.51
Beta-blocker	4 (44.4)	7 (43.8)	0.97
ACEI and/or ARB	8 (88.9)	10 (62.5)	**0.03***

Values are mean ± SD, n (%), or median (range). *p Values in bold indicates a statistically significant result.

ACS = acute coronary syndromes; ACEI = angiotensin-converting enzyme inhibitor ARB = angiotensin receptor blocker; BMI = body mass index; CAD = coronary artery disease; CK = creatine kinase; CK-MB = creatine kinase-myocardial band; HDL = high-density lipoprotein; LDL = low-density lipoprotein.

TABLE 2 Angiographic Findings and Plaque Distribution as Seen on OCT

	Patients With ACS (n = 9)	Patients w/o ACS (n = 16)	p Value*
Target vessel			
Left anterior descending artery	3 (33.3)	1 (6.3)	0.08
Left circumflex artery	1 (11.1)	2 (12.6)	0.92
Right coronary artery	5 (55.5)	0 (0)	**0.001***
No CAD	0 (0)	13 (81.3)	**0.001***
1-vessel disease	5 (55.5)	1 (6.3)	**0.001***
2-vessel disease	3 (33.3)	1 (6.3)	0.08
3-vessel disease	1 (11.1)	1 (6.3)	0.67
Percutaneous coronary intervention	9 (100)	3 (18.8)	**<0.001***
Plaque distribution on OCT			
Fibrotic plaque	1 (20.0)	4 (80.0)	0.06
- Pure fibrotic	0 (0)	2 (100)	
- Fibrocalcific	1 (33.3)	2 (66.6)	
Fibroatheroma	7 (36.8)	12 (63.2)	0.10
- Noncalcified	6 (42.9)	8 (57.1)	
- Calcified	1 (20.0)	4 (80.0)	
Thin-cap fibroatheroma	13 (59.1)	9 (40.9)	0.23
- Calcified TCFA	10 (62.5)	6 (37.5)	
- Noncalcified TCFA	3 (50.0)	3 (50.0)	

Values are n (%). *p Values in bold indicates a statistically significant result.

OCT = optical coherence tomography; TCFA = thin-cap fibroatheroma; other abbreviations as in Table 1 and 2.

in the coronaries (i.e., due to small vessel caliber and motion artifacts).

In patients with ACS, segments containing a culprit lesion (n = 11) showed significantly higher signal enhancement (CNR) following gadofosveset application than the remaining segments (n = 196) (CNR 6.1 [3.9 to 16.5] vs. 2.1 [0.5 to 3.5], respectively; p < 0.001). ROC analysis for the detection of culprit ACS lesions revealed an area under the curve of 0.870 (95% confidence interval [CI]: 0.780 to 0.960) with a sensitivity of 73% and specificity of 83%. The optimum cutoff value was found for a CNR of 4.7 (Figure 1A). Segmented areas of TCFA (n = 22) demonstrated a significantly higher CNR than segments without TCFAs (n = 185) (9.2 [3.3 to 13.7] vs. 2.1 [0.5 to 3.4], respectively; p < 0.001). Median CNR of TCFAs on pre-contrast scans was 1.3 (−0.8 to 6.2), differing significantly from post-contrast scans (9.2 [3.3 to 13.7]; (p < 0.001). There were no differences in CNR values between stable and TCFAs on the pre-contrast scans (2.1 [0.0 to 5.7] vs. 1.3 [−0.8 to 6.2], respectively; p = 0.372). ROC analysis revealed an area under the curve of 0.781 (95% CI: 0.654 to 0.909) with a sensitivity of 73% and specificity of 84% (Figure 1B). The optimum cutoff value was found for a CNR of 4.6.

There was a significant difference in signal intensity between culprit lesions in stable CAD patients and culprit lesions in ACS patients (3.2 [0.9 to 5.5] vs. 6.1 [3.9 to 16.5], respectively; p < 001) (Figure 2A) and between nonculprit ACS lesions and culprit ACS lesions (3.0 [1.3 to 4.5] vs. 6.1 [3.9 to 16.5], respectively; p < 0.001) (Figure 2B).

CMR SIGNAL ENHANCEMENT AMONG LOW (FIBROTIC), INTERMEDIATE (FIBROATHEROMA) AND HIGH-RISK PLAQUES (TCFA) ON OCT. All TCFAs (noncalcified and calcified; n = 22) were associated with significantly higher CNR values than all fibroatheromas (noncalcified and calcified; n = 19) (9.2 [3.3 to 13.7] vs. 3.1 [1.3 to 4.0], respectively; p < 0.001) and all fibrotic plaques (purely fibrotic and fibrocalcific; n = 5) (9.2 [3.3 to 13.7] vs. 1.1 [0.6 to 1.7], respectively; p < 0.001). In addition, slightly higher signal enhancement was observed at sites of fibroatheromas than at sites with fibrotic plaques; however,

FIGURE 1 **Median Signal Enhancement in Segments With Culprit ACS Lesions and Thin-Cap Fibroatheroma**

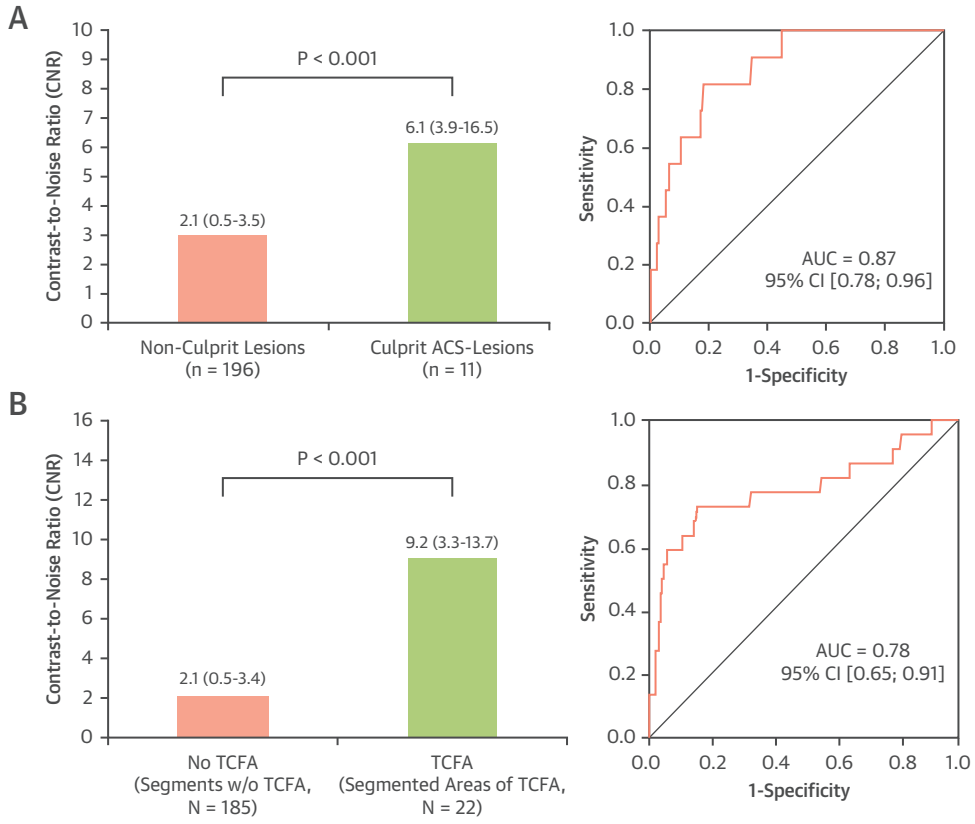

(A) Comparison of median signal enhancement between segments with (n = 11) and without (n = 196) an ACS-culprit lesion and corresponding ROC analysis. **(B)** Comparison of signal enhancement between segmented areas of TCFAs and segments with stable or no plaques and corresponding ROC analysis. ACS = Acute coronary syndromes; AUC = area under the curve; ROC = receiver operating curve; TCFA = thin-cap fibroatheroma.

they did not achieve statistical significance (3.1 [1.3 to 4.0] vs. 1.1 [0.6 to 1.7], respectively; p = 0.07) (Figure 2C).

CMR ANALYSIS II: BLINDED ANALYSIS FOR THE IDENTIFICATION OF CULPRIT ACS LESIONS. A CNR threshold of 4.7, which was determined by ROC analysis, allowed correct classification of 9 segments (sensitivity 82%) with and 162 segments (specificity 83%) without culprit coronary lesion (Figure 3).

OCT ANALYSIS. A total of 46 plaques were found during OCT analysis; 22 of 46 (47.8%) met the criteria of vulnerable plaques (i.e., noncalcified or calcified TCFA), whereas 24 of 46 coronary plaques (52.2%) were found to be stable. In 8 OCT pullbacks, corresponding to 10 coronary segments, no plaques were found. As a result, overall sites including stable plaques (n = 24) and nondiseased, healthy vessel walls (n = 10) there were n = 34 on OCT (Table 3). TCFA showed a significantly higher degree of luminal narrowing (46.5 ± 24.3% vs. 26.9 ± 17.3% stenosis) as assessed by XCA, whereas cap thickness was significantly lower in vulnerable plaques than in stable plaques (34.5 ± 13.9 μm vs. 96.8 ± 32.7 μm, respectively).

DISCUSSION

This study demonstrates for the first time a novel approach for detecting culprit coronary lesions in patients with ACS, which showed significantly higher gadofosveset uptake than segments with nonculprit coronary lesions or segments with healthy vessel walls. Additionally, in ACS and non-ACS patients, GE-CMR was able to identify TCFA with high diagnostic accuracy. GE-CMR may also have the ability to differentiate between low-risk (fibrotic), intermediate-risk (fibroatheroma), and high-risk (TCFA) coronary plaques, making GE-CMR a potential tool for cardiovascular risk stratification.

FIGURE 2 Comparison of Median Signal Enhancement Among Different Segments

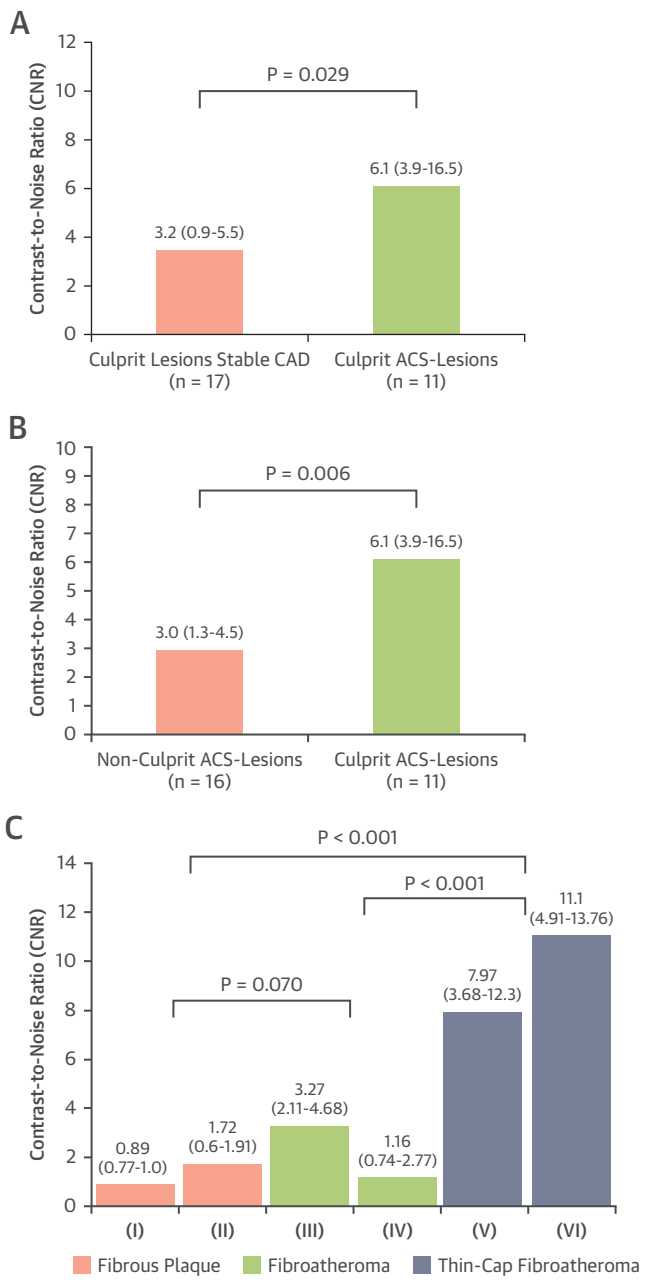

Comparison of median signal enhancement among **(A)** culprit lesions in stable CAD patients versus culprit ACS lesion; **(B)** nonculprit ACS lesions versus culprit ACS lesions; and **(C)** different plaque subtypes on GE-CMR. Type I fibrotic plaque (n = 2); CNR, 0.89 (range 0.77 to 1.0). Type II fibrocalcific plaque (n = 3): CNR, 1.72 (range 0.60 to 1.91. Type III noncalcified fibroatheroma (n = 14): CNR, 3.27 (range 2.11 to 4.68). Type IV calcified fibroatheroma (n = 5): CNR, 1.16 (range −0.74 to 2.77). Type V noncalcified TCFA (n = 16): CNR, 7.97 (range 3.68 to 12.30). Type VI calcified TCFA (n = 6): CNR, 11.10 (range 4.91 to 13.76). CAD = coronary artery disease; GE-CMR = gadofosveset-enhanced cardiac magnetic resonance; other abbreviations as in Figure 1.

FIGURE 3 ROC Curve for the Prediction of Culprit ACS Lesions

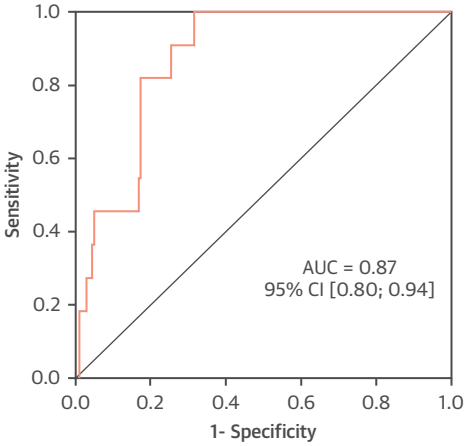

Blinded CMR evaluation (CMR analysis II) and corresponding ROC analysis. CMR = cardiac magnetic resonance; other abbreviations as in Figure 1.

INVASIVE IN VIVO DETECTION OF VULNERABLE ATHEROSCLEROTIC PLAQUE. In clinical practice, the visualization of coronary arteries has focused mainly on stenosis assessment by means of XCA. This luminographic technique, however, is not well suited for the evaluation of atherosclerotic plaques because vulnerable plaques in many cases do not cause significant luminal narrowing (1,13).

NONINVASIVE IMAGING OF CORONARY ATHEROSCLEROSIS BY CMR. Different CMR techniques have been used for noncontrast-enhanced and contrast-enhanced characterization of coronary atherosclerosis (14-16). For instance, noncontrast-enhanced T1-weighted CMR demonstrated potential for the detection of intraplaque hemorrhage and intracoronary thrombus (14,15,17). Contrast-enhanced CMR techniques enabled acquisition of additional information on plaque composition and biology (18,19). The potential of target-specific MR probes for biological characterization of coronary atherosclerosis, including fibrin-specific or elastin-specific probes, have also been demonstrated in experimental animal models and in humans (7,8,20).

ALBUMIN-SPECIFIC CMR FOR THE NONINVASIVE DETECTION OF CORONARY ATHEROSCLEROTIC PLAQUES. Gadofosveset is a target-specific molecular CMR imaging probe which binds to albumin and which has been approved for use in humans (7). Originally gadofosveset was designed as a blood pool

agent that allowed high-resolution steady-state angiography. However, later, its use was extended for imaging of endothelial permeability and neovascularization (7,21). Endothelial dysfunction, which is based on a reduced bioavailability of nitric oxide, results in impaired vasodilatation and increased endothelial permeability on the plaque surface. It plays a substantial role in atherogenesis and is an important predictor for future cardiovascular events (22). In inflamed atherosclerotic plaques, leaky endothelial junctions greater than 25 nm in diameter allow influx of low-density lipoproteins and macromolecules, such as albumin and leucocytes, into the vessel wall. This results in the progression of plaque development (22). Additionally, plaque growth is associated with intraplaque hypoxemia, leading to an

TABLE 3 Plaque Characterization on OCT

	TCFA (n = 22)	Stable Plaques and Nondiseased Coronary Sites (n = 34)	p Value*
MLA, mm^2	4.7 ± 3.9	6.1 ± 4.2	0.116
Lumen area proximal, mm^2	9.1 ± 4.8	9.1 ± 5.4	0.490
Lumen area distal, mm^2	7·5 ± 4.0	8.2 ± 5.3	0.319
Area stenosis, %	46.5 ± 24.3	26.9 ± 17.3	**<0.001***
Cap thickness, μm	34.5 ± 13.9	96.8 ± 32.7	**<0.001***
Lipid core	22 (100.0)	21 (61.7)	**<0.001***
Lipid core >180°	12 (54.5)	3 (8.8)	**<0.001***
Calcium	9 (40.9)	9 (26.5)	**0.259**
Thrombus	7 (31.8)	0 (0.0)	<0.001
Macrophage infiltration	6 (27.2)	4 (11.8)	0.900

Values are mean ± SD or n (%). *p Values in bold indicates a statistically significant result.
OCT = optical coherence tomography; MLA = minimal lumen area; TCFA = thin-cap fibroatheroma.

FIGURE 4 Sample Case 1

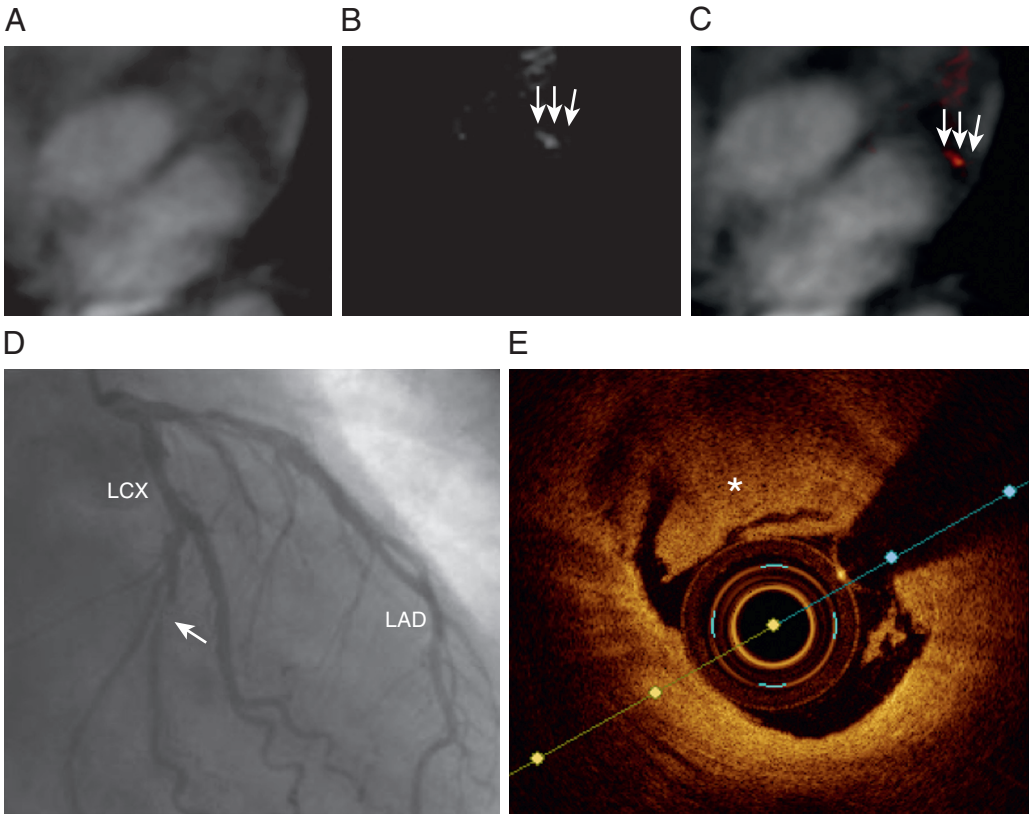

Data from a 51-year-old patient with NSTEMI. **(A)** CMR angiography demonstrates the location of the LCX. **(B)** Contrast enhancement **(white arrows)** in the LCX on GE-CMR. **(C)** To highlight the anatomic relationship between contrast enhancement and morphology, images were fused in a way similar to that with PET-CT. **(D)** X-ray coronary angiography depicts a significant stenosis in the mid-LCX as the culprit lesion **(white arrow)**, correlating with the increased signal intensity on GE-CMR. **(E)** OCT performed at the site of stenosis, demonstrates a plaque rupture with thrombus formation **(asterisk)**. CMR = cardiac magnetic resonance; GE-CMR = gadofosveset-enhanced cardiac magnetic resonance; LAD = left anterior descending artery; LCX = left circumflex artery; NSTEMI = non–ST-segment elevation myocardial infarction; OCT = optical coherence tomography; PET-CT = positron emission tomography-computed tomography.

FIGURE 5 Sample Case 2

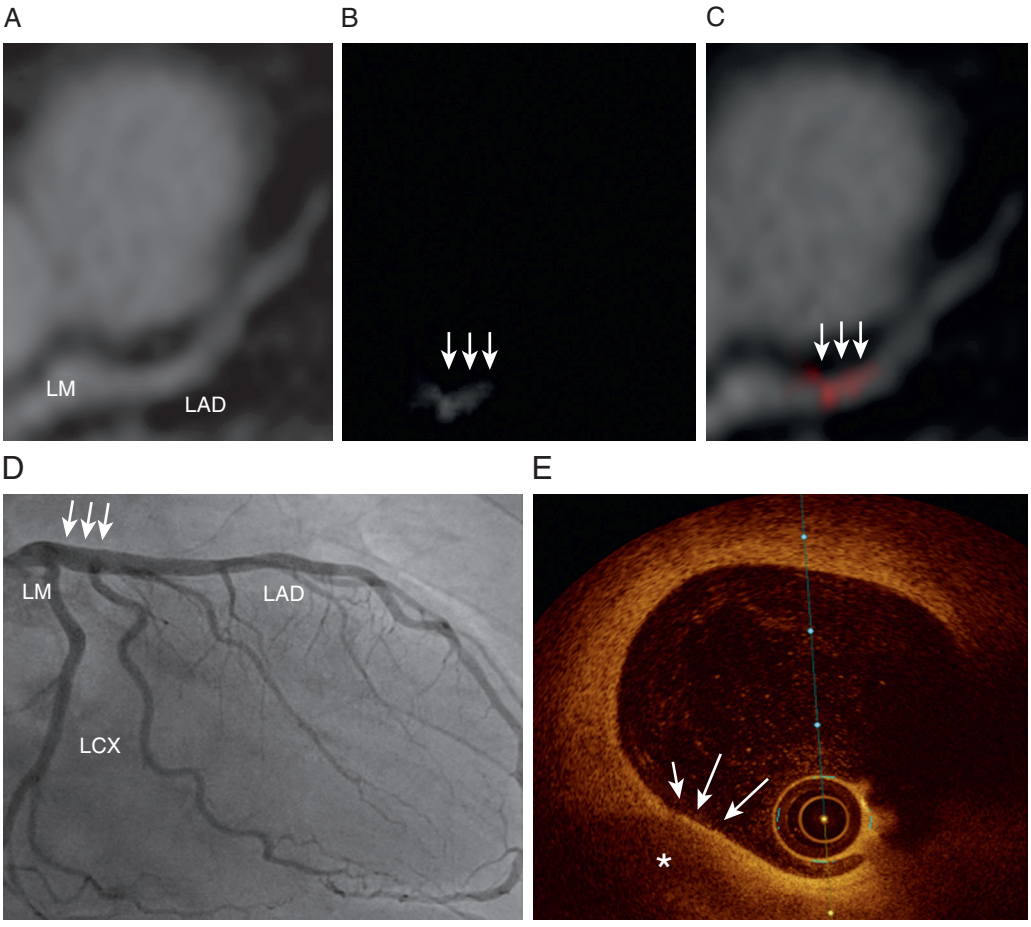

A 63-year-old patient with chest pain. **(A)** CMR angiography shows the course of the LM and LAD. **(B)** GE-CMR demonstrates contrast enhancement in the left main artery **(white arrows)**. **(C)** Fusion of CMR angiography and vessel wall imaging sequence. **(D)** XCA shows no signs of significant luminal narrowing in the entire coronary artery tree. **(E)** OCT reveals a thin-cap fibroatheroma **(white arrows)** with a large lipid core **(asterisk)** in the proximal LAD, correlating with the location of increased signal enhancement on GE-CMR. LM = left main; XCA = x-ray coronary angiography; other abbreviations as in Figure 4.

increase in neoangiogenesis and proliferation of new and fragile blood vessels with leaky endothelium, which are the main characteristic of vulnerable plaque (1-3). Lobbes et al. (7) observed a correlation between gadofosveset signal enhancement and the density of leaky neovessels in patients with symptomatic carotid artery disease.

A major goal of noninvasive cardiac imaging techniques is the early identification of unstable coronary artery plaques to prevent subsequent acute coronary events. Promising results regarding the detection of vulnerable plaque have been shown using morphological imaging techniques such as T1-weighted nonenhanced CMR, where differences in signal enhancement between vulnerable (plaques with high-intensity-positive signal) and stable plaques (lesions without high-intensity signal) were similar to those in our study. In addition to its potential to detect high-risk plaques, GE-CMR as a molecular imaging technique has the advantage that it is able to visualize a biological process that happens early in atherosclerotic plaque development and, therefore, may identify individuals with an increased risk of CAD at an early stage, who could benefit from pharmacologic treatment that aims to restore endothelium, such as the use of statins (23).

Importantly, conventional risk-scoring methods have not been able to clearly differentiate between patients who would profit from early coronary revascularization (i.e., type 1 myocardial infarction)

(Figure 4) and patients in whom optimization of medical therapy may be considered (i.e., type 2 myocardial infarction) (Figure 5). A noninvasive technique that can identify culprit lesions in ACS patients as suggested in our study, may therefore improve risk stratification and allow individually-tailored treatment.

STUDY LIMITATIONS. The relatively long scan time (28.6 ± 9.7 min for the baseline examination and 32 ± 7.9 min for the GE-CMR examination) may compromise the applicability of GE-CMR in a wide clinical setting. In the future, more advanced motion correction techniques (e.g., 100% scan efficiency) in combination with undersampled image reconstruction (e.g., compressed sensing) however, may help to overcome this limitation (24-27). In addition, the fusion of 2 data sets (CMR angiography and vessel wall imaging sequence) may suffer from misregistration errors and drifts due to the respiratory pattern of the patients, which could impair CMR analyses. New protocols and sequences which are currently under active investigation, may overcome this limitation (28,29). Plaques containing severe calcification may masquerade as TCFA, especially when the abluminal border of an area with a low signal cannot be visualized, and a bright band of fibrous tissue overlying the calcification appears as a thin fibrous cap (10). Moreover, the current trial was performed as a single-center study with a relatively small number of patients.

CONCLUSIONS

In this feasibility study, we demonstrated for the first time the noninvasive detection of culprit coronary lesions and thin-cap-fibroatheroma of the coronary arteries in vivo by using gadofosveset-enhanced CMR imaging. Signal enhancement 24 h following administration of gadofosveset may serve as a novel in vivo biomarker for the assessment of endothelial permeability and plaque instability.

ADDRESS FOR CORRESPONDENCE: Dr. Marcus Makowski, Department of Radiology and Cardiology, Charité Campus Benjamin Franklin, Universitätsmedizin Berlin, Hindenburgdamm Str. 30, D-12203, Berlin, Germany. E-mail: marcus.makowski@charite.de OR Dr. Boris Bigalke, Department of Radiology and Cardiology, Charité Campus Benjamin Franklin, Universitätsmedizin Berlin, Hindenburgdamm Str. 30, D-12203, Berlin, Germany. E-mail: boris.bigalke@charite.de.

PERSPECTIVES

COMPETENCY IN MEDICAL KNOWLEDGE: In vivo detection of TCFA and culprit coronary lesions using an albumin-binding MR probe is feasible in a "real world" patient population. GE-CMR may serve as a novel in vivo biomarker for endothelial permeability and plaque instability.

TRANSLATIONAL OUTLOOK: Based on this imaging method, early diagnosis and characterization of coronary atherosclerotic plaque may help to initiate adequate preventative measures such as an intensified statin therapy or coronary intervention. Larger studies are needed to assess whether gadofosveset-enhanced CMR improves risk stratification and clinical outcome in CAD patients.

REFERENCES

1. Otsuka F, Joner M, Prati F, Virmani R, Narula J. Clinical classification of plaque morphology in coronary disease. Nat Rev Cardiol 2014;11:379-89.

2. Virmani R, Burke AP, Kolodgie FD, Farb A. Vulnerable plaque: the pathology of unstable coronary lesions. J Interv Cardiol 2002;15:439-46.

3. Virmani R, Kolodgie FD, Burke AP, Farb A, Schwartz SM. Lessons from sudden coronary death: a comprehensive morphological classification scheme for atherosclerotic lesions. Arterioscler Thromb Vasc Biol 2000;20:1262-75.

4. Makowski MR, Wiethoff AJ, Blume U, et al. Assessment of atherosclerotic plaque burden with an elastin-specific magnetic resonance contrast agent. Nat Med 2011;17:383-8.

5. Judenhofer MS, Wehrl HF, Newport DF, et al. Simultaneous PET-MRI: a new approach for functional and morphological imaging. Nat Med 2008;14:459-65.

6. Makowski MR, Preissel A, von Bary C, et al. Three-dimensional imaging of the aortic vessel wall using an elastin-specific magnetic resonance contrast agent. Invest Radiol 2012;47:438-44.

7. Lobbes MB, Heeneman S, Passos VL, et al. Gadofosveset-enhanced magnetic resonance imaging of human carotid atherosclerotic plaques: a proof-of-concept study. Invest Radiol 2010;45:275-81.

8. Phinikaridou A, Andia ME, Protti A, et al. Noninvasive magnetic resonance imaging evaluation of endothelial permeability in murine atherosclerosis using an albumin-binding contrast agent. Circulation 2012;126:707-19.

9. Roffi M, Patrono C, Collet JP, et al. 2015 ESC guidelines for the management of acute coronary syndromes in patients presenting without persistent ST-segment elevation: Task Force for the Management of Acute Coronary Syndromes in Patients Presenting without Persistent ST-Segment Elevation of the European Society of Cardiology (ESC). Eur Heart J 2016;37:267-315.

10. Kini AS, Vengrenyuk Y, Yoshimura T, et al. Fibrous cap thickness by optical coherence tomography in vivo. J Am Coll Cardiol 2017;69:644-57.

11. Prati F, Regar E, Mintz GS, et al. Expert review document on methodology, terminology, and clinical applications of optical coherence tomography: physical principles, methodology of image acquisition, and clinical application for assessment of coronary arteries and atherosclerosis. Eur Heart J 2010;31:401-15.

12. Cheng JM, Garcia-Garcia HM, de Boer SP, et al. In vivo detection of high-risk coronary plaques by

radiofrequency intravascular ultrasound and cardiovascular outcome: results of the ATHEROREMO-IVUS study. Eur Heart J 2014;35:639–47.

13. Tian J, Dauerman H, Toma C, et al. Prevalence and characteristics of TCFA and degree of coronary artery stenosis: an OCT, IVUS, and angiographic study. J Am Coll Cardiol 2014;64:672–80.

14. Jansen CH, Perera D, Makowski MR, et al. Detection of intracoronary thrombus by magnetic resonance imaging in patients with acute myocardial infarction. Circulation 2011;124:416–24.

15. Hoshi T, Sato A, Akiyama D, et al. Coronary high-intensity plaque on T1-weighted magnetic resonance imaging and its association with myocardial injury after percutaneous coronary intervention. Eur Heart J 2015;36(29):1913–22.

16. Noguchi T, Kawasaki T, Tanaka A, et al. High-intensity signals in coronary plaques on noncontrast T1-weighted magnetic resonance imaging as a novel determinant of coronary events. J Am Coll Cardiol 2014;63:989–99.

17. Noguchi T, Tanaka A, Kawasaki T, et al. Effect of intensive statin therapy on coronary high-intensity plaques detected by noncontrast T1-weighted imaging: the AQUAMARINE pilot study. J Am Coll Cardiol 2015;66:245–56.

18. Mavrogeni S, Markousis-Mavrogenis G, Koutsogeorgopoulou L, et al. Cardiovascular magnetic resonance imaging pattern at the time of diagnosis of treatment naive patients with connective tissue diseases. Int J Cardiol 2017;236:151–6.

19. Storz C, Hetterich H, Lorbeer R, et al. Myocardial tissue characterization by contrast-enhanced cardiac magnetic resonance imaging in subjects with prediabetes, diabetes, and normal controls with preserved ejection fraction from the general population. Eur Heart J Cardiovasc Imaging 2017 Jul 26 [E-pub ahead of print].

20. Andia ME, Saha P, Jenkins J, et al. Fibrin-targeted magnetic resonance imaging allows in vivo quantification of thrombus fibrin content and identifies thrombi amenable for thrombolysis. Arterioscler Thromb Vasc Biol 2014;34:1193–8.

21. Pedersen SF, Thrysoe SA, Paaske WP, et al. CMR assessment of endothelial damage and angiogenesis in porcine coronary arteries using gadofosveset. J Cardiovasc Magn Reson 2011;13:10.

22. Davignon J, Ganz P. Role of endothelial dysfunction in atherosclerosis. Circulation 2004;109 Suppl 1:III27–32.

23. Treasure CB, Klein JL, Weintraub WS, et al. Beneficial effects of cholesterol-lowering therapy on the coronary endothelium in patients with coronary artery disease. N Engl J Med 1995;332:481–7.

24. Pang J, Sharif B, Arsanjani R, et al. Accelerated whole-heart coronary MRA using motion-corrected sensitivity encoding with three-dimensional projection reconstruction. Magn Reson Med 73:284–91.

25. Cruz G, Atkinson D, Buerger C, Schaeffter T, Prieto C. Accelerated motion corrected three-dimensional abdominal MRI using total variation regularized SENSE reconstruction. Magn Reson Med 2016;75:1484–98.

26. Piccini D, Littmann A, Nielles-Vallespin S, Zenge MO. Respiratory self-navigation for whole-heart bright-blood coronary MRI: methods for robust isolation and automatic segmentation of the blood pool. Magn Reson Med 2012;68:571–9.

27. Luo J, Addy NO, Ingle RR, et al. Nonrigid motion correction with 3D image-based navigators for coronary MR angiography. Magn Reson Med 2017;77:1884–93.

28. Xie Y, Kim YJ, Pang J, et al. Coronary atherosclerosis T1-weighted characterization with integrated anatomical reference: comparison with high-risk plaque features detected by invasive coronary imaging. J Am Coll Cardiol Img 2017;10:637–48.

29. Ginami G, Neji R, Phinikaridou A, Whitaker J, Botnar RM, Prieto C. Simultaneous bright- and black-blood whole-heart MRI for noncontrast enhanced coronary lumen and thrombus visualization. Magn Reson Med 2017 Jul 19 [E-pub ahead of print].

KEY WORDS atherosclerosis, CMR, endothelial dysfunction, molecular imaging, vulnerable plaque

APPENDIX For expanded methods, please see the online version of this paper.

View publication stats